

## **CHAPTER 5**

### **FLOOD PREDICTION USING MICROWAVE REMOTE SENSING**

#### **5.1 INTRODUCTION**

Flood is a natural phenomenon, which can be predicted using scientific methods. Use of remote sensing in flood prediction is common among the remote sensing utilities. However, the use of any such prediction mechanism using microwave remote sensing is possible only with the customisation, based on local conditions. Keeping this point in view, the present study attempts to see possible utility of microwave remote sensing for prediction of flood.

Following flood prediction methods developed are explained in the subsequent sections.

- (a) Flood prediction based on characteristic changes of microwave polarization index.
- (b) Flood prediction based on precipitation data obtained from microwave remote sensors.
- (c) Flash flood prediction based on observation of cloud having potential for cloudburst, relating to microwave radiation parameters.

The chapter is organised as the following. Section 5.2 and 5.3 present two case studies of flood prediction using polarization index computed in X-band. This is followed

by the techniques of flood prediction using microwave remote sensed precipitation data demonstrated for two more cases in section 5.4 and 5.5 respectively. In section 5.6 a novel technique of flash flood prediction using cloudburst forecasting is presented using passive microwave brightness temperature difference. Finally the chapter is concluded in section 5.7.

## **5.2 MONITORING POLARIZATION INDEX IN THE UPSTREAM OF RIVER BRAHMAPUTRA FOR FLOOD PREDICTION IN LOWER BASIN OF THE VALLEY**

### **5.2.1 Introduction**

The river Brahmaputra flows through the state of Assam in India for a total length of 916 km. Every year during monsoon season, typically from May to October, the overflowing river water creates heavy flood in large portions of the valley. The present study utilizes polarization index ( $PI$ ) derived from microwave brightness temperature ( $T_B$ ) at 10 GHz for predicting flood in the Brahmaputra valley.

A need for such kind of a study was felt based on various reports of human lives lost seen to happen every year during flood in Assam, due to lack of proper flood prediction mechanism. The damages caused by flood over the years in Assam are shown in Figure 5.1. A microwave remote sensing based flood prediction mechanism is expected to help reduce such damages to a great extent.

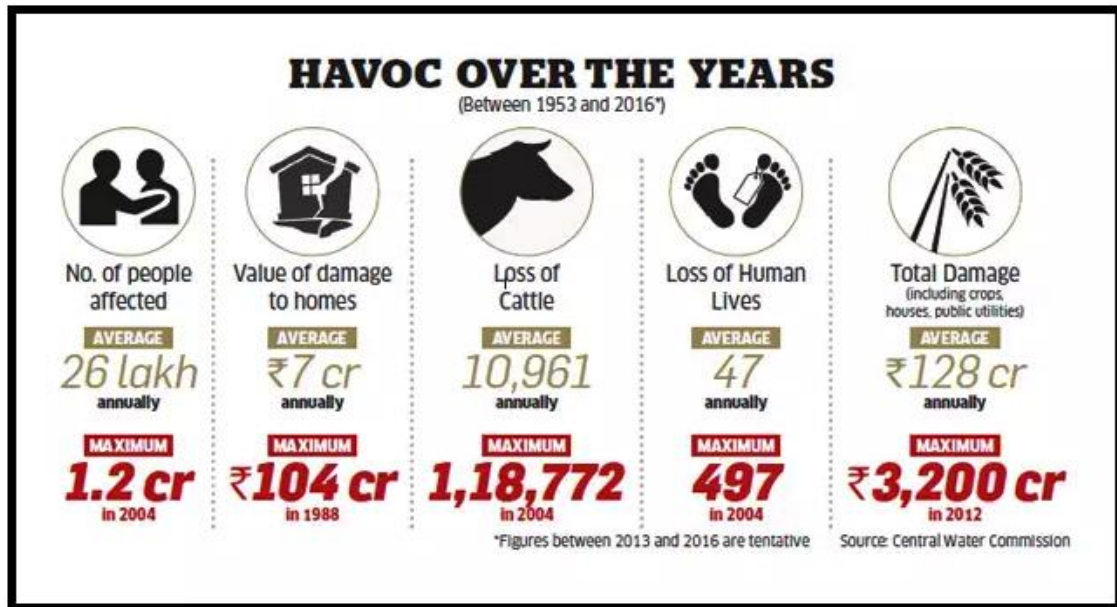


Figure 5.1: Damages caused by flood over the years in Assam [Source: *Central Water Commission*]

### 5.2.2 Theoretical Background

Passive microwave remote sensed polarization index ( $PI$ ) and its use have been explained in Chapter 1. The change in the value of  $PI$  takes place with the change in soil moisture or water expanse in an area. An attempt has been made to use this phenomenon for predicting flood in the region of study.

### 5.2.3 Equipments and Data Used

Following are the equipments and data used for the study.

- (a) A PC with the 'Beam VISAT' software for data analysis.
- (b) Brightness Temperature data in 10 GHz frequency, in both horizontal and vertical polarizations obtained from AMSR 2 sensor of GCOM-W1 satellite.

### 5.2.4 Study Area

The area selected for detection of water expanse changes around the river Brahmaputra is the region surrounded by  $27.75^{\circ}$  to  $28.5^{\circ}$  N latitude and  $95.45^{\circ}$  to  $95.75^{\circ}$  E longitude. The map of the area is shown in Figure 5.2.



Figure 5.2: Area for monitoring of *PI* value for flood prediction

Flood prediction using the method described in this section has been tested for Kaziranga National Park and South Kamrup of Assam.

### 5.2.5 Experiments Done

The brightness temperature values for the area shown in Figure 5.2 are monitored for the whole monsoon season. Then the *PI* values are computed from the brightness temperatures. The *PI* values are then averaged for the whole area. The variation of the

average  $PI$  value is then observed in a graphical form. The observed  $PI$  variation gives the indication regarding possible flooding in the valley downstream of the river.

### 5.2.6 Results and Discussion

The variation of the average value of  $PI$  computed as explained in the previous section for the period of 1<sup>st</sup> August to 15<sup>th</sup> September of 2015 is shown in Figure 5.3.

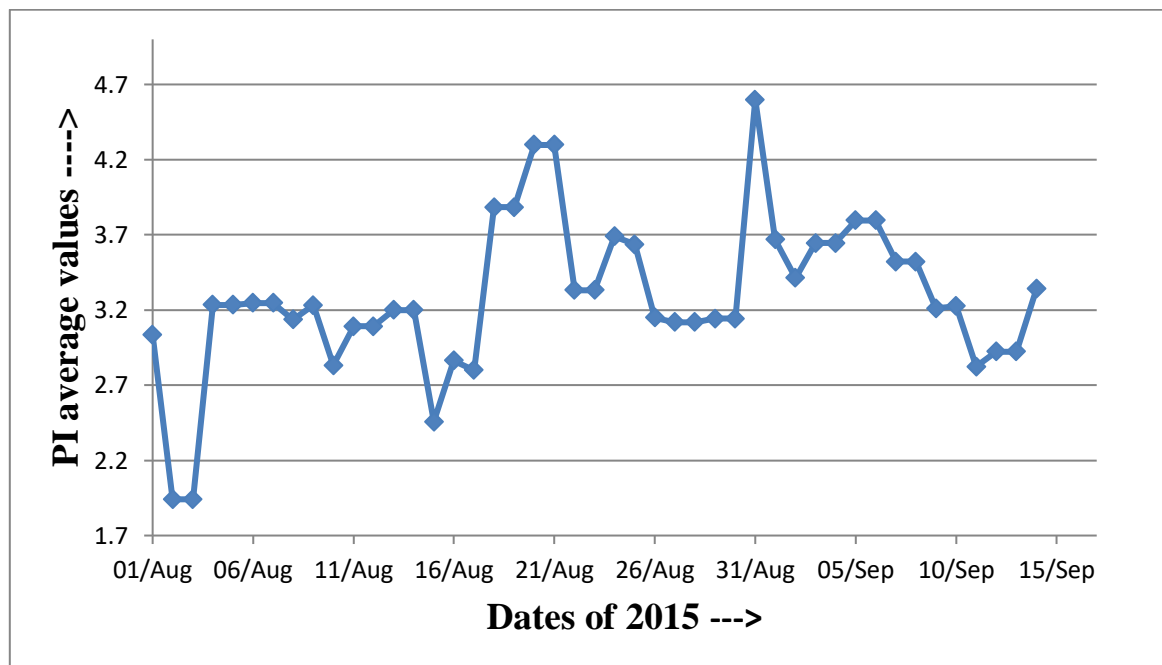


Figure 5.3: Variation of  $PI$  average values during August-September 2015

High peak of averaged  $PI$  values are observed around Brahmaputra near Sadia on 20<sup>th</sup> and 21<sup>st</sup> August and then on 31<sup>st</sup> August 2015. Subsequent to these dates, actual flood occurrences are reported in the whole of Brahmaputra valley as per ASDMA reports [64].

### 5.2.7 Observation on time-lag of real occurrence of flood in the downstream areas for validation

Figures 5.4 and 5.5 show maps of an area of the Kaziranga National Park as on 22<sup>nd</sup> and 23<sup>rd</sup> August 2015, obtained from Bhuvan portal of ISRO. Figure 5.4 shows the area having no flood (2 days after the high value of average *PI* appears) and Figure 5.5 shows flooding spots by light blue patches on the map (3 days after the high value of average *PI* appears).



Figure 5.4: Bhuvan image of Kaziranga National Park on 22<sup>nd</sup> August 2015 shows no flood

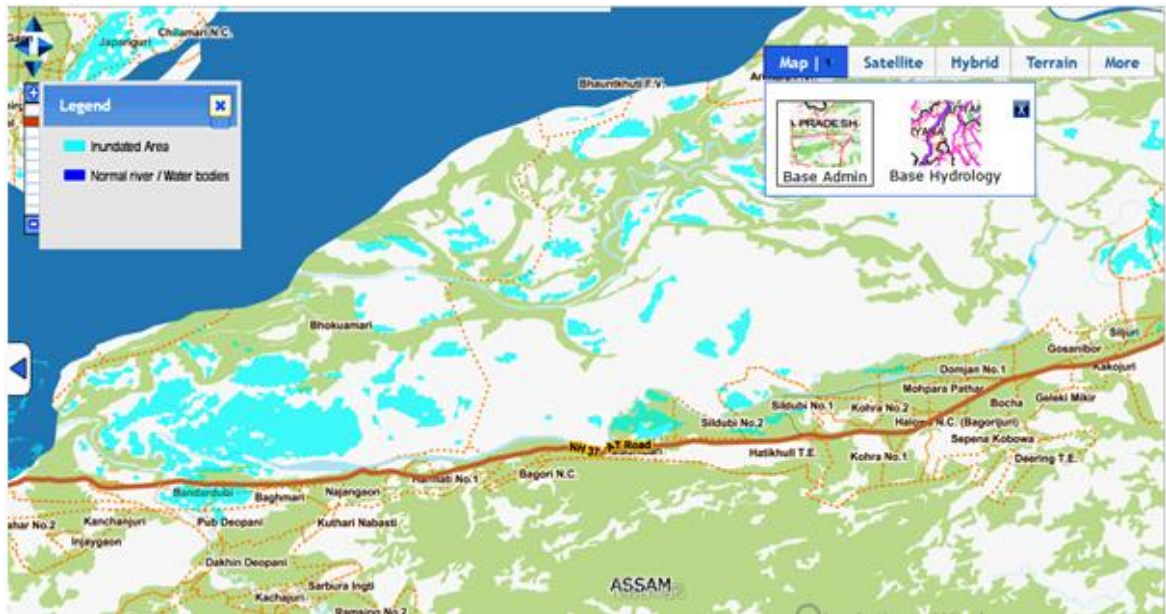


Figure 5.5: Bhuvan image of Kaziranga National Park on 23<sup>rd</sup> August 2015 shows flooding spots

Similarly, on 2<sup>nd</sup> September 2015, i.e., two days after the indication by high value of average  $PI$  (on 31<sup>st</sup> August 2015) is obtained (as shown in Figure 5.3), flooding occurs at Kaziranga National Park, as shown by the flood map obtained from Bhuvan portal, shown in Figure 5.6.

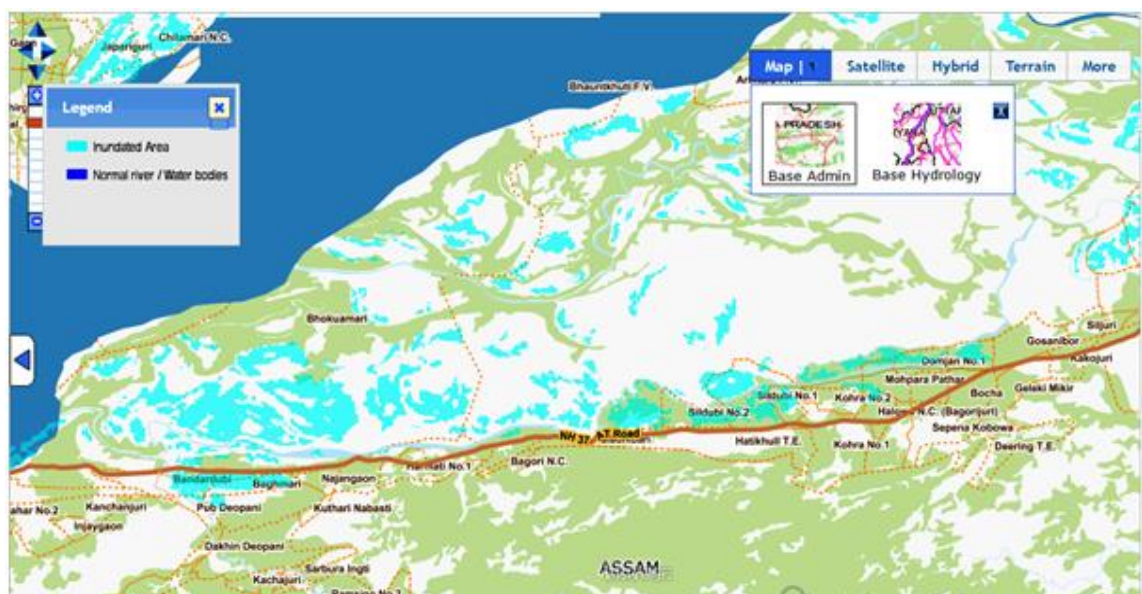


Figure 5.6: Bhuvan image of Kaziranga National Park on 2<sup>nd</sup> September 2015 shows flooding spots

Again after the flood receded, in the image of 6<sup>th</sup> September 2015 no flooding is observed in that same area, as seen from Figure 5.7. This signifies that the peak (high) value of average *PI* occurs only before the occurrence of major flood of larger spatial extent, as validated also by comparing with the Bhuvan images. The flood occurrence dates are validated also with ASDMA daily flood report data which show the same results as the Bhuvan flood maps.



Figure 5.7: Bhuvan image of Kaziranga National Park on 6<sup>th</sup> September 2015 shows no flood

The flood occurrence in South Kamrup area of Brahmaputra valley is also correlated with the same average *PI* and similar results are obtained.

The Bhuvan maps of South Kamrup area on different dates of August and September 2015 show that major floods have actually occurred after there was advanced indication in the form of appearance of peaks of the average *PI* values computed near Sadia area on and near the river Brahmaputra. The dates of high peak values of *PI* and the dates of actual occurrences of flood in South Kamrup are listed in the following.

The above validation shows that the high peak value of  $PI$  occurs only before flooding. Before non flooding days, this  $PI$  value remains normal, as seen from Figure 5.3.

For the years 2014 and 2016 also similar results are obtained from Bhuvan images. Thus the high  $PI$  average value ( $\geq 3.8$ ) measured for the selected area (around Sadia) gives an early indication of major floods in various downstream regions of the Brahmaputra valley in the whole state of Assam. The results of several such flooding events during 2014-2016 are correlated with ASDMA reports, for drawing authentic inferences. Figures 5.8 to 5.10 show the relationships of  $PI$  variations with the flooded crop areas as per ASDMA reports, for the years 2014, 2015 and 2016 respectively.

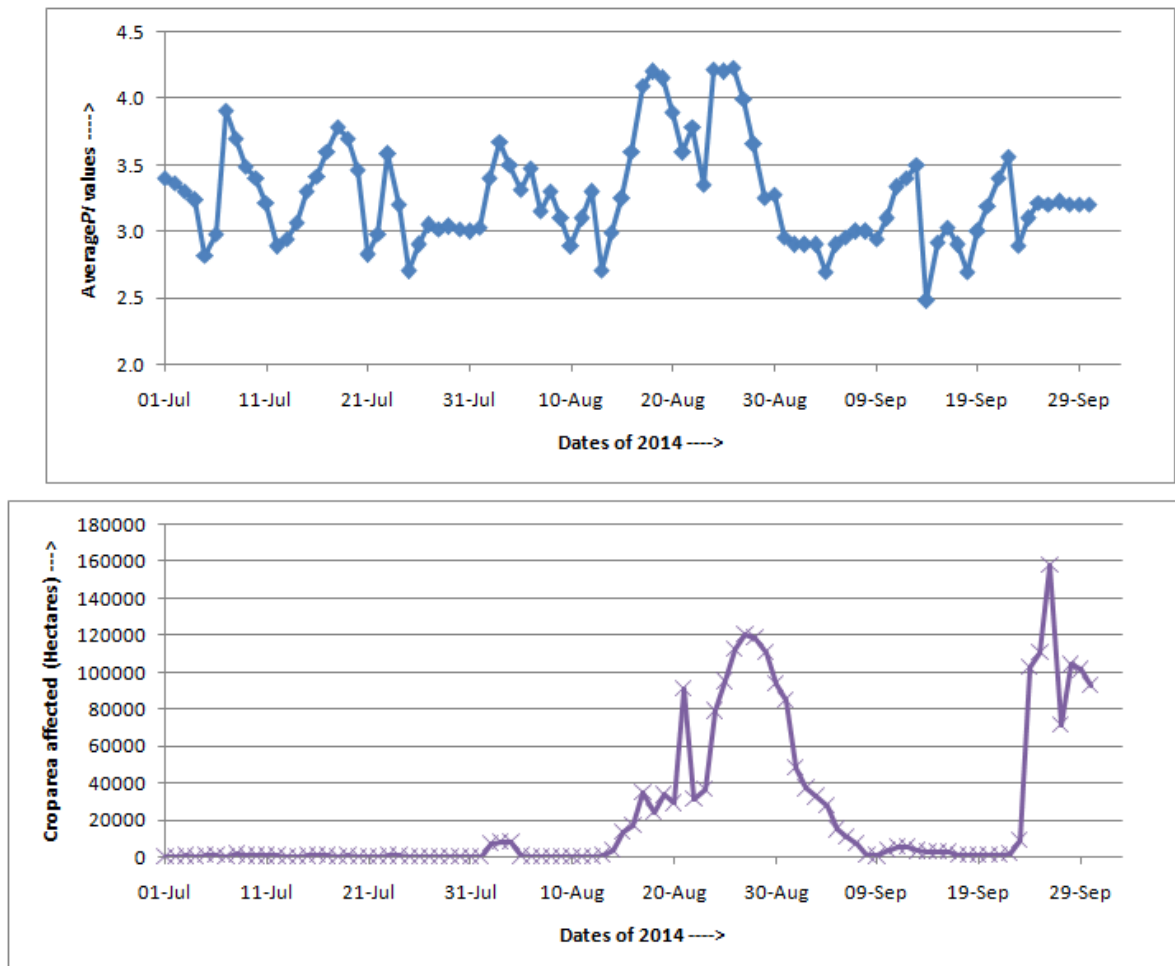


Figure 5.8: Variations of computed average  $PI$  and flood affected crop area as per ASDMA report in the Brahmaputra valley in 2014

As seen in Figure 5.8 the sharp peaks of calculated  $PI$  values precede the peak flooding dates in the later part of August and early September in 2014 by 2-3 days. However, the similar variations are not seen in case of high flood in the later part of September. This is due to the fact that the areas found flooded during 22-26 September 2014 in Assam were not inundated due to Brahmaputra river overflow. Rather those areas were deluged due to heavy local precipitation including cloudburst, leading to flash flood [68]. This shows the potential of using microwave data for flood prediction effectively, but with consideration of local conditions.

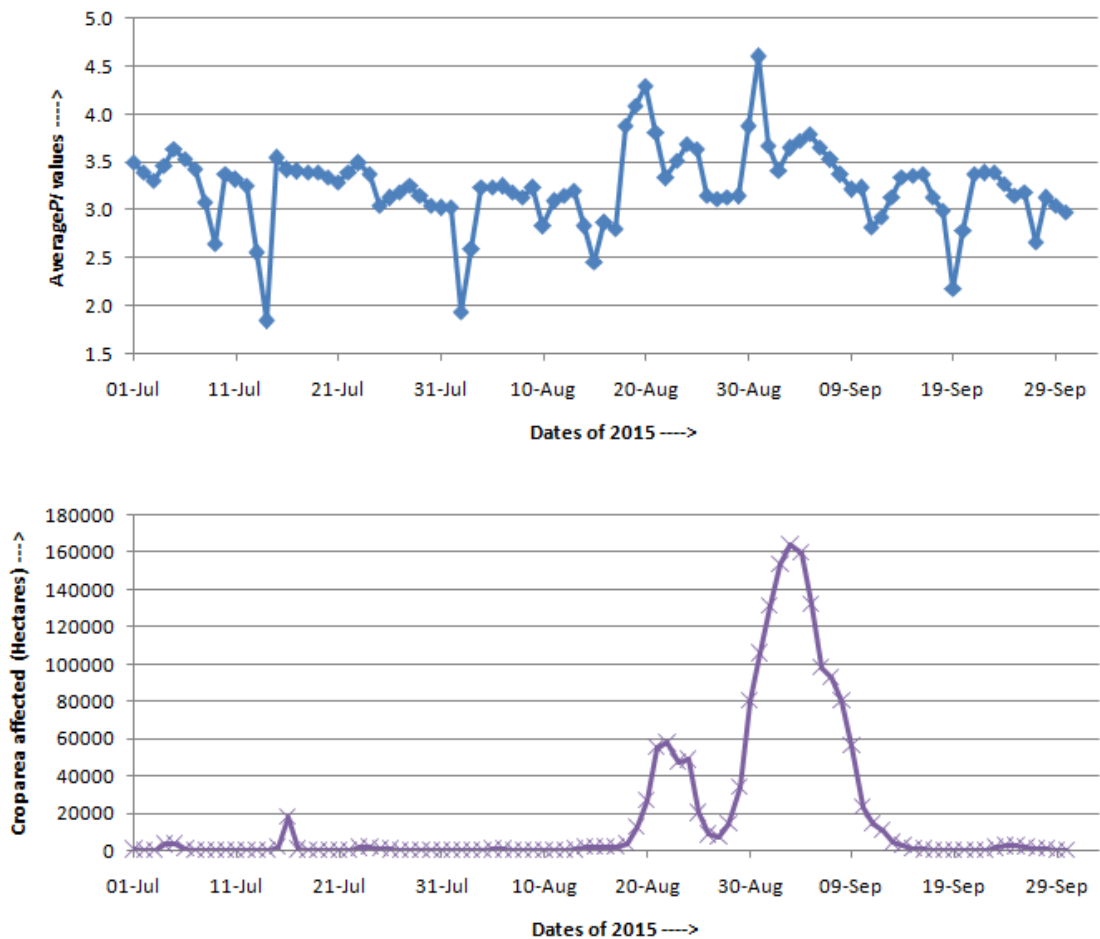


Figure 5.9: Variations of computed average  $PI$  and flood affected crop area as per ASDMA report in the Brahmaputra valley in 2015

Next, as observed from Figure 5.9 the sharp peaks of calculated  $PI$  values precede the peak flooding dates in August and September 2015 by 2-3 days. This shows the

potential of using microwave data for flood prediction effectively, without any error in some seasons.

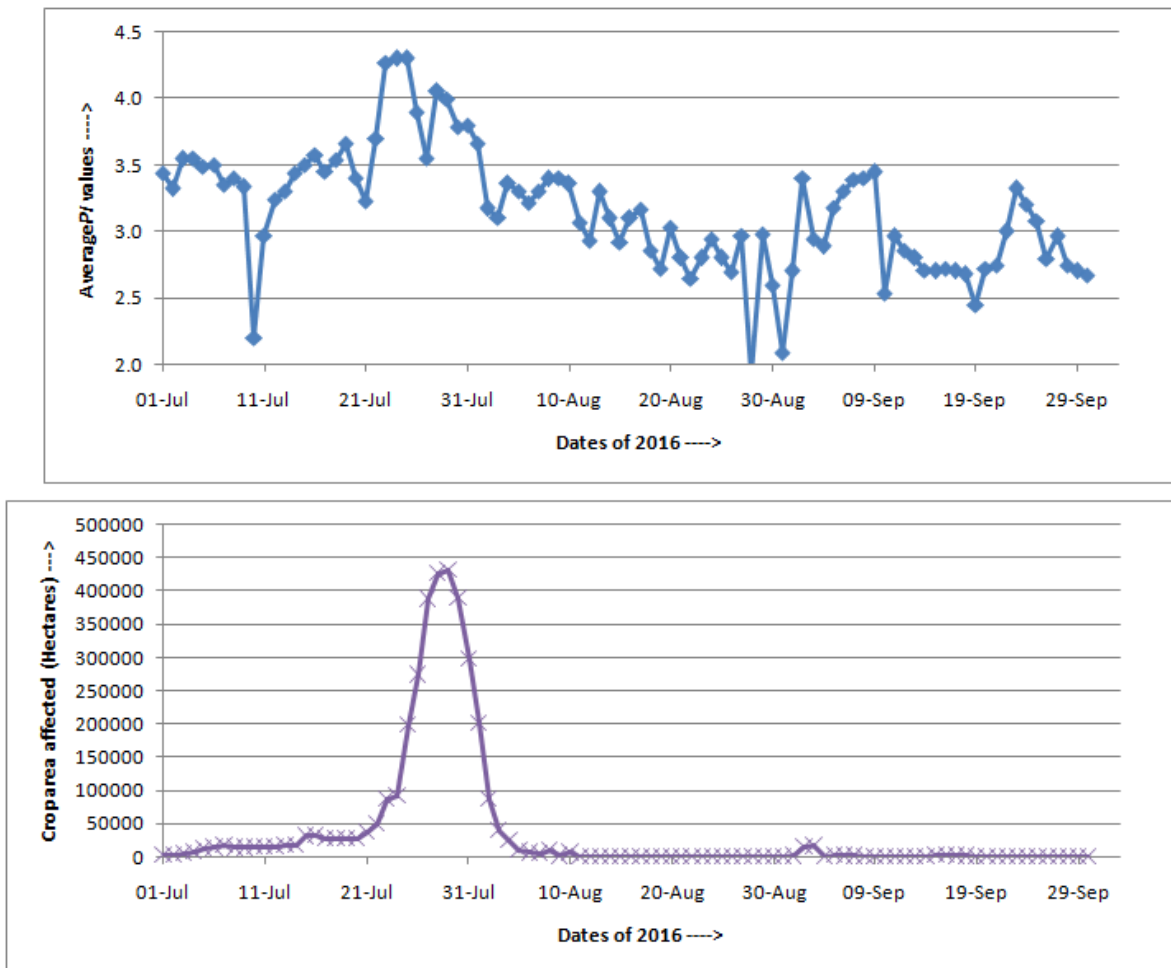


Figure 5.10: Variations of computed average  $PI$  and flood affected crop area as per ASDMA report in the Brahmaputra valley in 2016

Again in Figure 5.10 it is observed that the sharp peaks of calculated  $PI$  values above a normal level precede the peak flooding dates in August and September 2016 by 2-3 days. This observation also validates the potential of using microwave data for flood prediction effectively, without any error in some seasons.

### **5.2.8 Inferences**

The correlations of the experimental results with the flood reports from ASDMA and the flood images from Bhuvan portal show the validity and accuracy of the method in predicting flood. Monitoring of the average *PI* value of an area upstream of a river for flood prediction downstream is a novel idea. It gives accuracy close to 80 percent, in predicting major flood in the Brahmaputra valley. However, use of local conditions and ancillary data may make the accuracy higher in predicting flood using the methodology described here.

## **5.3 MONITORING POLARIZATION INDEX IN THE BOUNDARY AREA OF THE RIVER BRAHMAPUTRA FOR FLOOD PREDICTION IN MORIGAON DISTRICT**

### **5.3.1 Introduction**

Brahmaputra is the largest river of India and flows through the state of Assam over a length of 916 km. The river causes flood in many places in the valley along its length during monsoon season. The district of Morigaon in Assam is one of the highly flood affected districts in the state, primarily caused by overflow of river water in the Brahmaputra. The prediction of these events of flooding using conventional optical remote sensing is often not possible due to cloud cover over these regions throughout the monsoon season. Hence, passive microwave remote sensing is used in the present work to monitor the changes in expanse of river water over the Brahmaputra near Morigaon district.

### **5.3.2 Theoretical Background**

Polarization index (*PI*) derived from passive microwave brightness temperature in X-band acts as the indicative parameter for monitoring the river water expanse. As

described in the previous section, the use of *PI* in 10 GHz frequency makes it possible to monitor the soil moisture and water expanse levels in the area of study considered.

### **5.3.3 Equipments and Data Used**

Following are the equipments and data used for the study.

- (a) A PC with the 'Beam VISAT' software for data analysis.
- (b) Brightness Temperature data in 10 GHz frequency, in both horizontal and vertical polarizations obtained from AMSR 2 sensor of GCOM-W1 satellite.

### **5.3.4 Study Area**

The area of study selected for applying the methodology is the district of Morigaon in the state of Assam in India, having a total area of 1450 sq. kms. The district boundaries are- the river Brahmaputra on the North, Karbi Anglong district on the South, Nagaon district on the east and Kamrup district on the west. The map of the district is shown in Figure 5.11. The district boundary ranges in world geographic coordinates as- Longitude ranging from 91.96° E to 92.56° E, Latitude ranging from 26.06° N to 26.50° N.



Figure 5.11: Morigaon District [Sources: [www.mapsofindia.com](http://www.mapsofindia.com) and google maps]

The exact study area in the brightness temperature image is shown in the form of the pixels in the map in Figure 5.12, with rectangular boxes. The coordinates of the pixels are shown in Table 5.1 in terms of latitude and longitude for each pixel number.

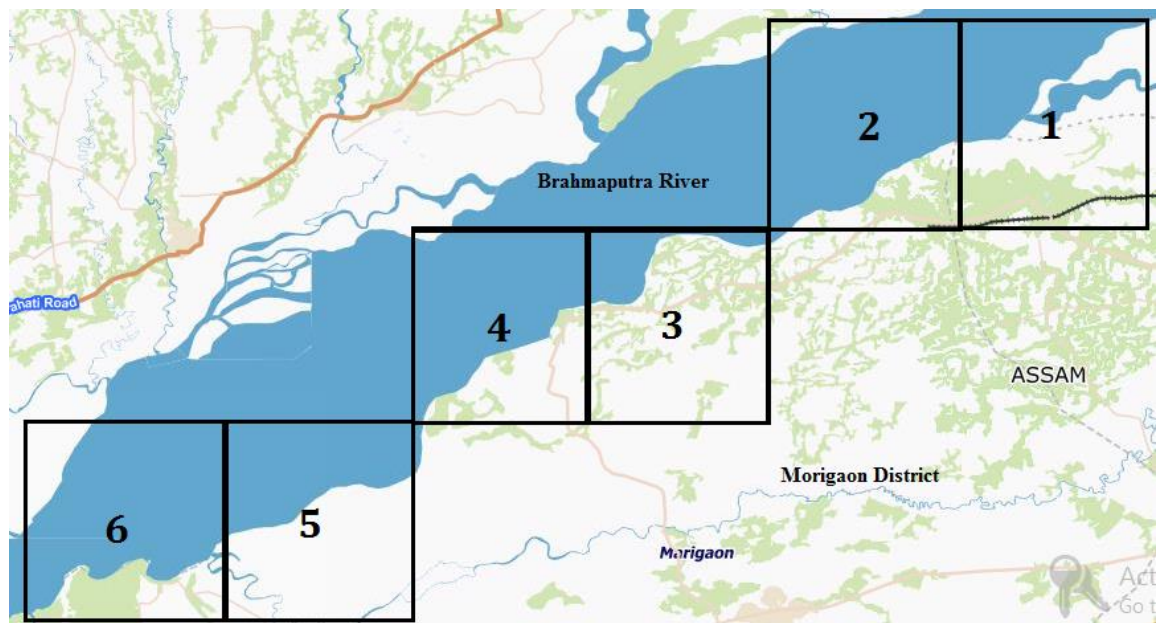


Figure 5.12: Pixels chosen for computing  $PI$  average values [Map source: Bhuvan portal of ISRO]

Table 5.1: Longitudes and Latitudes of Pixels chosen for *PI* computation

Pixel No.	Longitude (°E)	Latitude (°N)
1	92.5	26.5
2	92.4	26.5
3	92.3	26.4
4	92.2	26.4
5	92.1	26.3
6	92.0	26.3

### 5.3.5 Experiments Done

The methodology of the work is based on the measurement of *PI* over the river Brahmaputra for six boundary pixels of Morigaon district and taking average of the values. Table 5.2 shows a sample set of  $T_B$  values, both in horizontal and vertical polarizations, during the descending pass for a day that is two days before a major flood in Morigaon. The *PI* calculated for the day and the average *PI* are also shown in the same table.

Table 5.2: Sample values of  $T_B$ , *PI* and average *PI* for 5<sup>th</sup> of August, 2015

Pixel No.	$T_B$ at Horizontal Polarization (K)	$T_B$ at Vertical Polarization (K)	Polarization Index ( <i>PI</i> )	Average <i>PI</i>
1	202.14	245	9.6	9.9
2	218.3	255.41	7.8	
3	184.5	234.96	12.0	
4	203.4	247	9.7	
5	185.3	233.65	11.5	
6	209.9	248.91	8.5	

The district of Morigaon is in the south bank of the river Brahmaputra and overflow of the river causes flood every monsoon season. Monitoring of the pixels as shown in Figure 5.12 can indicate the slow progression of rising water level, finally resulting in the overflowing condition to cause flood, and thus can act as an early warning for flooding in the district.

### 5.3.6 Experimental Results and Validation Done

The results obtained from the *PI* calculations are correlated with the daily flood reports obtained from Assam State Disaster Management Authority (ASDMA), a government agency of the state of Assam, India. ASDMA reports are based on physical survey of the places done on real time basis. The Figures 5.13 and 5.14 show the comparison of *PI* values with the total crop area affected (in Hectares) for the district of Morigaon on corresponding dates of 2015 and 2016 respectively.

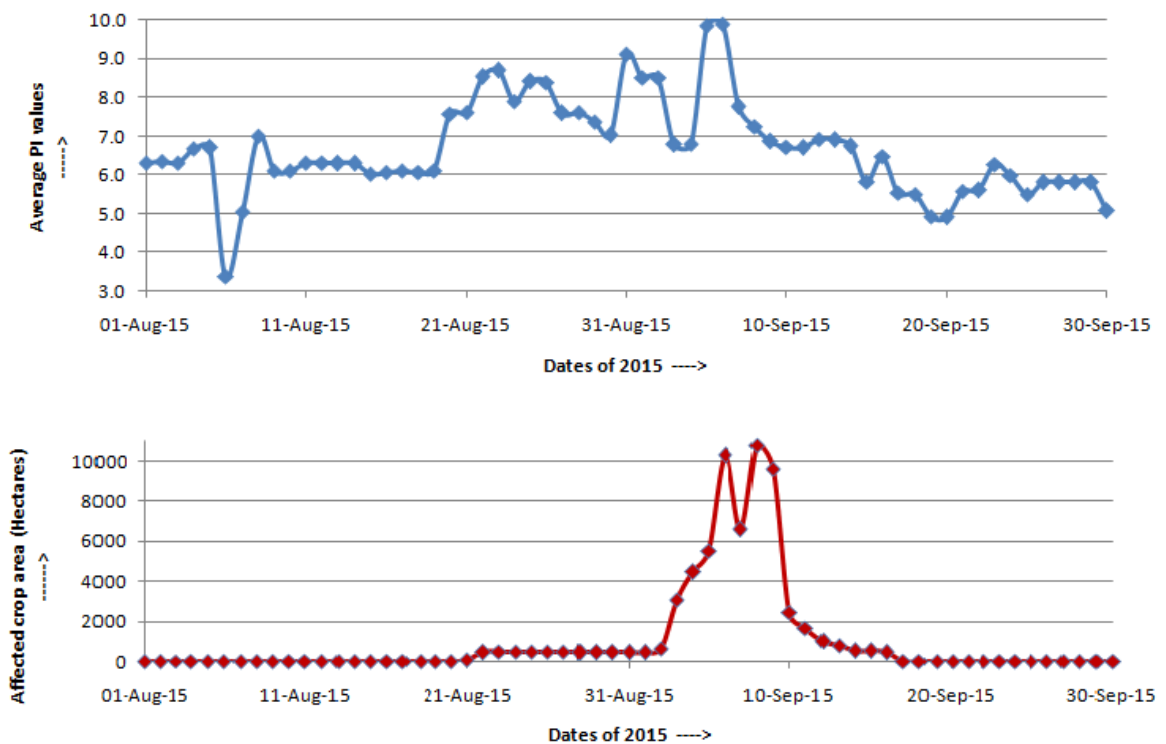


Figure 5.13: Variation of average *PI* values and crop area affected in 2015

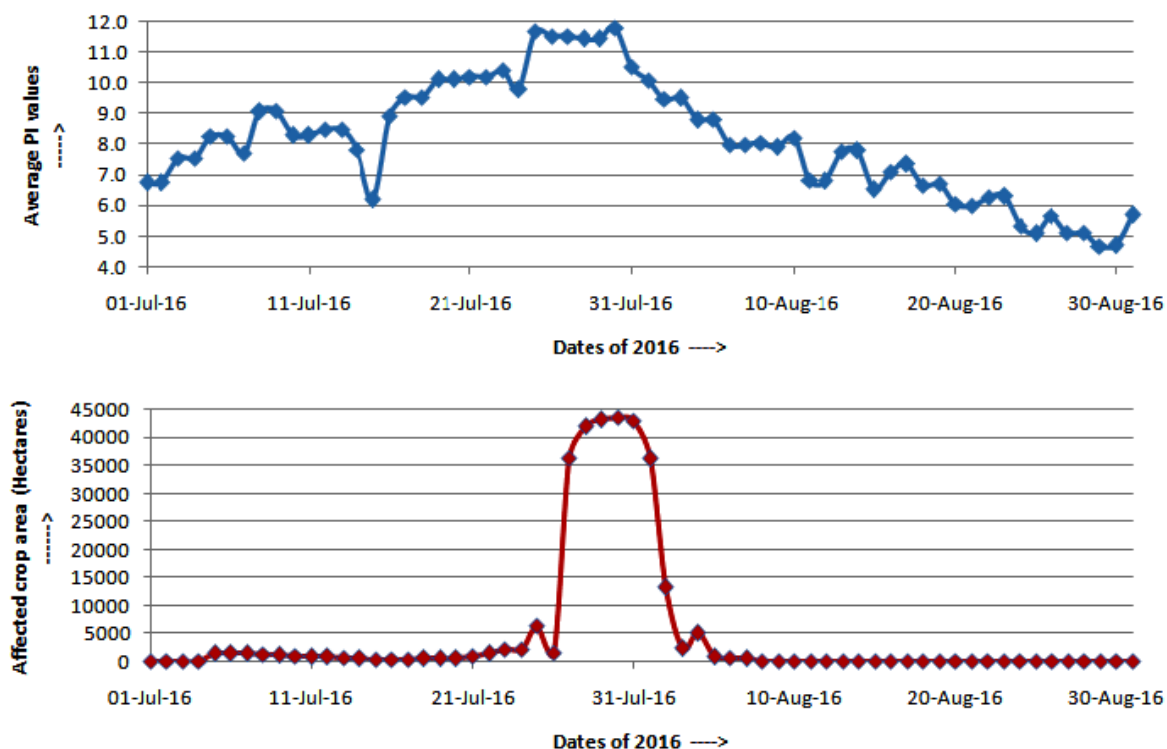


Figure 5.14: Variation of average *PI* values and crop area affected in 2016

The Figure 5.16 shows a high value of computed average *PI* crossing 9.0 on 31<sup>st</sup> August 2015, indicating a steep rise in the value due to increase in water cover within the pixels, due to overflowing river Brahmaputra. Correspondingly from 3<sup>rd</sup> September onwards the magnitude of flood increases manifold in the district. This is observed from the increase in crop area affected, in the same figure. The graph shows that the crop area affected by flood increases from 445 Hectares on 31<sup>st</sup> August to 3102 Hectares on 3<sup>rd</sup> September 2015. The *PI* shows high values intermittently till 6<sup>th</sup> September, reaching the highest value of 9.9 and then decreasing gradually from 7<sup>th</sup> September onwards. From 9<sup>th</sup> September onwards the *PI* values are less than 7. Correspondingly the crop area affected also decreases gradually and becomes zero by 17<sup>th</sup> September, 2015.

Similar trend is observed for the year 2016 also. The Figure 5.14 shows the trend of rise and decline of the average *PI* values and the corresponding record of crop area affected by flood in Morigaon district in 2016. 17<sup>th</sup> July 2016 onwards the *PI* value remains high (> 9). Correspondingly from 21<sup>st</sup> July onwards the crop area affected by flood

increases and rises to as high as 43,602 Hectares on 30<sup>th</sup> July. From 1<sup>st</sup> August onwards the average *PI* value decreases steeply. Correspondingly the crop area affected by flood also decreases gradually and becomes zero on 8<sup>th</sup> August, 2016.

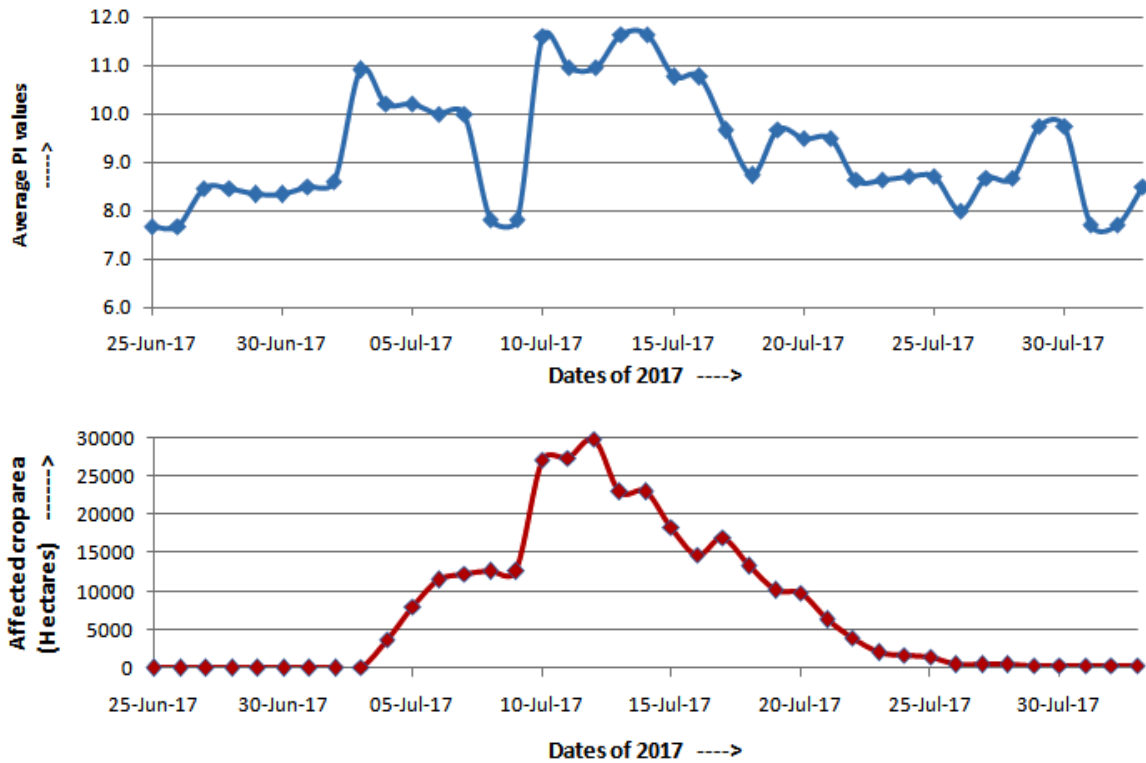


Figure 5.15: Variation of average *PI* values and crop area affected in July 2017

The developed methodology is also applied to predict flood in Morigaon district for the flood that occurred in July 2017. Figure 5.15 shows the results of that analysis. High peak values of average *PI* are found to occur from 3<sup>rd</sup> to 7<sup>th</sup> July and again from 10<sup>th</sup> to 16<sup>th</sup> July 2017. Correspondingly the occurrence of high magnitude flood is seen in the form of crop area affected from 4<sup>th</sup> July onwards, having peak magnitude from 10<sup>th</sup> to 14<sup>th</sup> July. The flood prediction methodology is thus validated.

### 5.3.7 Inferences

The average *PI* gives an indication of the river water expanse along Morigaon district. The increase in water expanse in that area over the river and its bank leads to high

magnitude flood in Morigaon. A threshold value of the average *PI* therefore can be fixed as 9.0, such that whenever this value is crossed, there is possibility of high magnitude flood in the district of Morigaon within a period of 1 - 4 days. This lead time of flood prediction can be useful in sending alert to the vulnerable areas in the district.

The methodology is tested for three consecutive years from 2015 to 2017. However the technique needs to be tested also for other places near rivers, where major flooding is caused due to river overflow. The methodology discussed in this section can be a useful alternative to existing remote sensing based techniques for prediction of flood, when cloud cover hinders the use of existing conventional optical remote sensing based techniques. The accuracy level obtained in predicting flood by this method is close to 80 percent. However, use of many other local factors such as precipitation, water level of other rivers and tributaries of the Brahmaputra etc. may improve the efficiency of the method used.

## **5.4 FLOOD PREDICTION IN THE DOWNSTREAM AREAS OF BRAHMAPUTRA VALLEY BY USING PRECIPITATION DATA FROM MICROWAVE REMOTE SENSING SATELLITE**

### **5.4.1 Introduction**

During the monsoon season in India, floods occur due to heavy rainfall. But floods sometimes also result from storm surge, associated with a tropical cyclone, a tsunami or a high tide, coinciding with higher than normal river water levels. In the Brahmaputra valley in the state of Assam, incessant heavy rainfall in the upstream of the river also causes inundation in the downstream areas on both sides of the river. Real time monitoring of precipitation upstream can therefore be an important activity in predicting flood downstream. This technique of monitoring precipitation for flood prediction in the Brahmaputra valley is described in the subsequent sub-section.

### **5.4.2 Theoretical Background**

The precipitation affects the microwave signals reaching the sensor on board the satellite, from the earth. Heavy precipitation attenuates the signals significantly. The attenuation level is therefore proportional to the amount of precipitation. This attenuation level is used to measure the amount of precipitation by several algorithms and thus ready precipitation data is available from microwave satellites. Also the signal scattering that takes place due to the water droplets of the rainfall gives indication regarding the extent of rainfall. From such multiple phenomena the precipitation level that is derived is available for the users to download from the passive microwave remote sensing data providing websites.

### **5.4.3 Equipments and Data Used**

For the present work, precipitation data is obtained from Advanced Microwave Scanning Radiometer (AMSR) 2 on board Global Change Observation Mission (GCOM) W1 satellite of Japan Aerospace Exploration Agency (JAXA). It is also understood that this real time data obtained, if timely utilized, can help in providing aids to decrease the human mortality rate. In the downloaded microwave remote sensed precipitation image, the amount of precipitation in mm/h is available pixel-wise.

For analysing the precipitation images of the satellite, the ‘Beam-VISAT’ software obtained from European Satellite Agency (ESA) is used. The results of the analysis are then exported to spread-sheets for further calculations.

### **5.4.4 Study Area**

In the present study an algorithm is developed to assess the total precipitation values measured along both northern as well as southern banks of the river Brahmaputra, in the areas upstream of the Kaziranga National Park in Assam. The measurement area

extends up to 50 kilometres in both northern and southern banks of the river. The study area is shown in the map in Figure 5.16.



Figure 5.16: Points of precipitation measurement on and around the river Brahmaputra

The precipitation values are obtained for the months of August and September, 2014. The historical flood record according to Assam State Disaster Management Authority (ASDMA) also show that the districts of Assam affected severely by flood during August and September, 2014 are Dhemaji, Jorhat, Lakhimpur, Sivasagar, Tinsukia, Nagaon, Golaghat, Barpeta, Bongaigaon, Sonitpur, Morigaon, Dibrugarh, Kamrup, Goalpara, Nagaon, Nalbari, Kokrajhar, Dhubri, Darrang, Karbi Anglong and Chirang. Out of all these places, in the present study the devastating floods which happened in the Kaziranga National Park area in Golaghat district was considered for prediction and analysis.

The tables as well as the graphs show the total precipitation values obtained for the places extending from 93.3°E to 95.6°E and 26.5°N to 27.8°N.

### 5.4.5 Experiments Done

The values of precipitation for a particular place on a day can be found directly from the precipitation map of AMSR-2. By placing pins for a particular latitude and longitude on that place, the amount of precipitation for that place recorded by AMSR-2 sensor in mm/hr can be obtained.

The methodology as shown in Figure 5.17 utilizes the sum of the values of the precipitation data obtained from a large upstream area of the Brahmaputra valley, for prediction of flood downstream. If the sum crosses a certain threshold, flood occurs in the downstream areas. This way the precipitation data of the upstream areas of Brahmaputra valley can be used for forecasting of flood in the low lying areas of the Kaziranga national park, situated downstream of the valley.

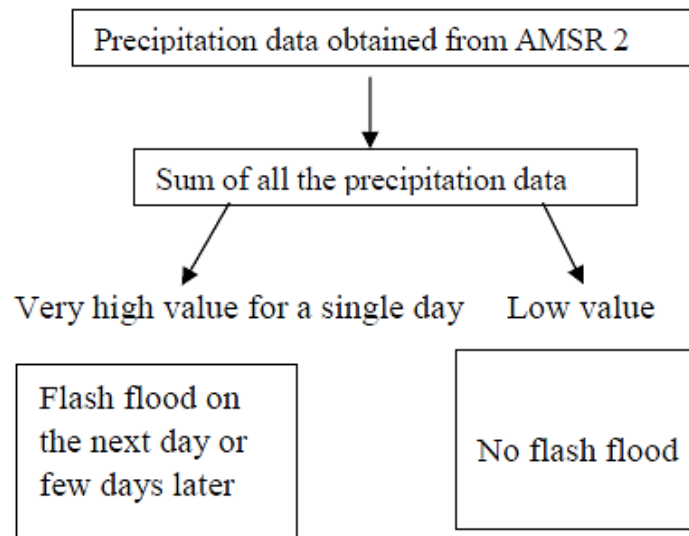


Figure 5.17: Methodology used for prediction of flood in Assam

### 5.4.6 Results and Discussion

Table 5.3 and 5.4 show the precipitation values obtained from descending and ascending passes of the satellite, for the places upstream of Kaziranga National Park. Figures 5.18 and 5.19 show the variations of the sum of precipitation values for the places considered, during descending and ascending passes of the satellite respectively.

Table 5.3: Precipitation values (in mm/hr) obtained from AMSR 2 with respect to descending pass for the month of August 2014, upstream of Kaziranga National Park

Sl. No.	Places	Dates of August 2014									
		10	12	13	14	15	17	20	21	22	24
1	Jengraimukh	0	54	630	0	0	0	0	0	0	0
2	North Lakhimpur	0	515	485	0	0	0	0	0	0	0
3	Bihpuria	0	45	278	0	0	0	0	280	0	0
4	Harmuti	0	31	805	0	0	0	0	96	0	0
5	Jonai	0	786	405	114	0	7	0	46	0	0
6	Simen Chapori	0	48	76	122	33	0	680	0	0	0
7	Majuli	0	26	0	0	0	0	0	0	28	0
8	Narayanpur	0	0	212	0	9	0	0	0	0	1799
9	Gohpur	0	0	173	0	0	0	0	5037	0	0
10	Behali	0	0	0	0	0	0	0	476	0	0
11	Dhakuakhana	149	0	0	0	0	0	498	0	0	0
12	Dhemaji	268	0	597	0	10	0	997	0	0	0
13	Silapathar	848	0	660	0	70	0	49	0	0	0
14	Chapakhowa	0	365	141	151	107	178	0	0	0	492
15	Doom Doma	264	115	0	71	1	0	0	0	0	0
16	Tinsukia	0	24	0	31	0	0	0	0	0	0
17	Chabua	0	93	0	0	0	0	0	71	0	0
18	Dibrugarh	0	0	88	0	0	0	433	0	0	0
19	Sibsagar	144	0	0	0	230	0	0	315	0	0
20	Gaurisagar	0	0	10	0	31	0	0	0	0	0
21	Chenijaan	0	0	0	0	13	0	0	0	0	0
22	Rajahauli	0	0	0	0	13	0	0	0	0	0
23	Dergaon	0	44	61	0	2	0	0	0	0	0
24	Rajabari	0	57	0	0	0	0	0	74	0	0
25	Bokakhat	0	283	0	0	0	0	0	463	0	0
26	Tilikiam	0	0	48	0	2	0	0	0	25	0
27	Kaziranga	0	0	0	36	0	0	0	199	0	0
28	Haladhibari	0	0	0	22	0	0	0	0	0	0
29	Kohora	0	0	0	22	0	0	0	0	0	0
30	Sepon	0	0	0	0	25	0	0	0	0	0
31	River Brahmaputra	5	38	160	60	25	0	0	0	0	0

32	River Brahmaputra	0	419	346	69	0	0	0	43	0	0
33	River Brahmaputra	0	915	0	69	0	0	0	59	0	0
34	River Brahmaputra	0	125	216	47	70	0	532	0	0	0
Sum of all precipitation values (mm)		1678	3983	5391	814	641	185	3189	7159	53	2291

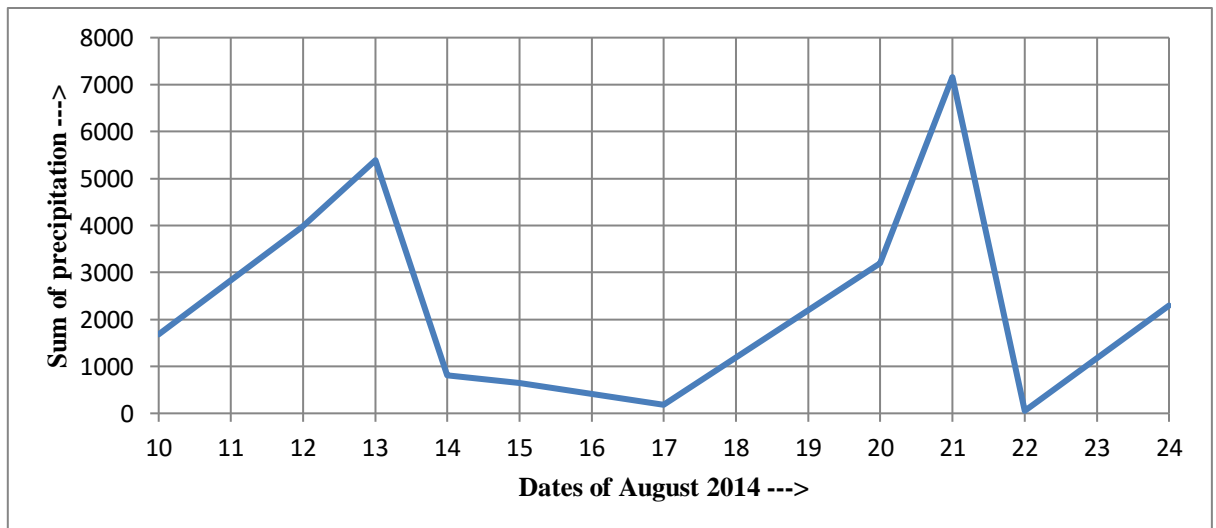


Figure 5.18: Sum of precipitation values obtained for the places upstream of Kaziranga area during descending pass of the satellite

Table 5.4: Precipitation values (in mm/hr) obtained from AMSR 2 with respect to descending pass for the month of August, 2014, upstream of Kaziranga National Park

Sl. No.	Places	Dates of August 2014									
		12	13	14	15	18	23	24	25	27	29
1	Jengraimukh	0	0	870	0	0	0	0	0	0	0
2	North Lakhimpur	0	0	0	0	0	0	0	0	0	0
3	Bihpuria	0	0	58	0	0	0	0	0	0	0
4	Harmuti	0	0	55	0	0	0	0	0	0	0
5	Jonai	0	0	71	0	0	46	0	996	0	0

6	Simen Chapori	0	0	204	0	0	0	0	689	0	0
7	Majuli	0	0	0	0	0	0	0	0	0	0
8	Narayanpur	0	0	48	13	0	0	0	0	0	0
9	Gohpur	0	0	61	0	0	0	54	0	0	0
10	Behali	0	0	75	0	0	0	0	0	0	0
11	Dhakuakhana	0	0	360	0	0	0	0	42	0	0
12	Dhemaji	0	0	253	0	0	0	0	191	0	0
13	Silapathar	0	0	300	0	0	0	0	629	31	0
14	Chapakhowa	96	0	0	0	0	474	0	0	0	0
15	Doom Doma	37	0	0	0	116	0	0	88	0	0
16	Tinsukia	0	0	0	0	0	0	0	130	0	0
17	Chabua	0	0	0	0	9	0	0	349	0	0
18	Dibrugarh	0	0	320	0	0	0	0	689	0	0
19	Sibsagar	0	0	75	0	0	0	0	0	0	0
20	Gaurisagar	0	0	45	0	0	0	0	0	0	0
21	Chenijaan	0	0	0	0	0	0	0	0	0	0
22	Rajahauli	0	0	0	0	0	0	0	0	0	0
23	Dergaon	0	0	40	0	0	0	0	0	0	0
24	Rajabari	0	0	46	0	187	0	0	0	0	0
25	Bokakhat	0	0	45	0	0	0	0	0	0	0
26	Tilikiam	0	0	28	0	0	0	0	0	0	0
27	Kaziranga	0	0	0	0	0	0	149	0	0	0
28	Haladhibari	0	0	68	0	0	0	0	0	0	0
29	Kohora	0	0	68	0	0	0	0	0	0	0
30	Sepon	0	0	0	0	0	0	0	0	0	0
31	River Brahmaputra area1	28	0	0	0	0	692	0	253	0	0
32	River Brahmaputra area2	0	0	70	0	0	71	0	626	0	0
33	River Brahmaputra area3	0	0	214	0	0	0	0	494	0	0
Sum of all precipitation values (mm)		161	0	3374	13	312	1283	203	5176	31	0

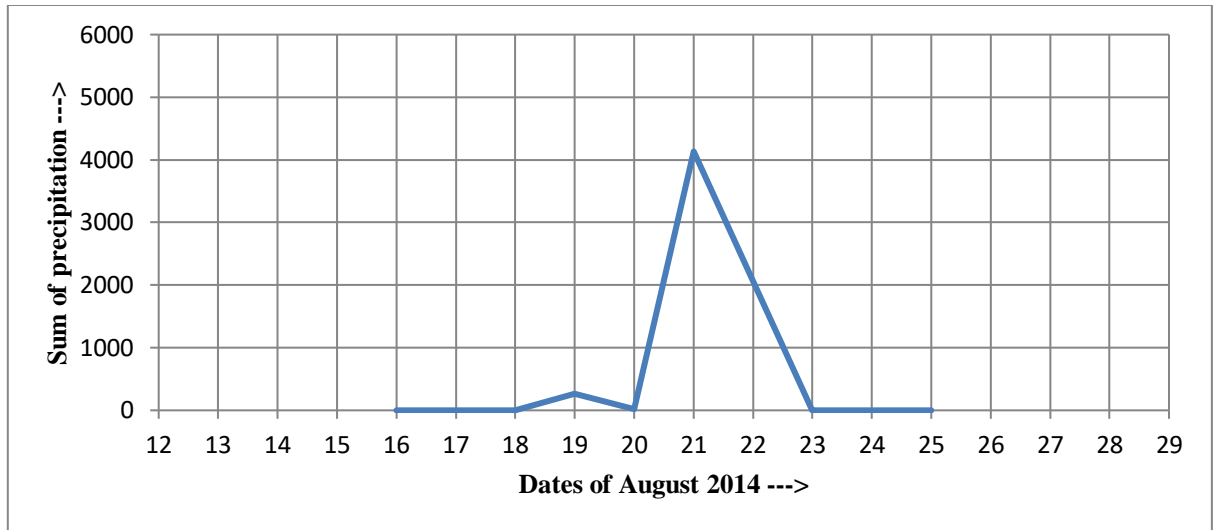


Figure 5.19: Sum of precipitation values obtained for the places upstream of Kaziranga area during ascending pass of the satellite

From the precipitation data of AMSR-2 it is noted that on 21<sup>st</sup> of August 2014, a very high total precipitation value of 5037 mm/h and on 24<sup>th</sup> of August a total of 1799 mm/h precipitation value are recorded for the upstream areas along the course of the Brahmaputra.

All the places where high values of precipitation are observed are located upstream in the valley. This has caused rise in the water level of the river Brahmaputra and subsequently caused more water flowing down along the course of the river. This high quantity water flow down the river causes flood downstream.

#### 5.4.7 Validation

The validation of the methodology of prediction of flood is done by comparing the results of prediction with the actual flood occurrences in the targeted area, i.e., Kaziranga National Park. On 15<sup>th</sup> of August, 2014, almost 50% and on 23<sup>rd</sup> August, more than 70% of land area of Kaziranga was reported to be inundated, as per Assam State Disaster Management Authority (ASDMA) flood report. On 28<sup>th</sup> of August one adult rhino and one

hog deer were reported to be dead in floodwater. The timely detection and forecasting of flood could have possibly led to evacuation operations, causing less damage to the people, livestock and wild animals. Hence, the methodology as proposed and experimental results thereof are found to be correct in predicting the occurrence of major flood in the Kaziranga National Park area.

#### **5.4.8 Inferences**

It is seen that a simple methodology of selection of an area in the microwave remote sensing image, for obtaining precipitation information, and then calculating the sum of precipitation can lead to successful prediction of flood in the Brahmaputra valley. This method is thus useful in predicting the flood in the downstream low lying areas of a river, by computing the sum of precipitation upstream, using microwave remote sensed precipitation data. The advantage of using microwave data in this case is the availability of average precipitation information twice daily for a large area of 25 km x 25 km. This makes the use of such data very convenient for precipitation calculations and subsequent applications in flood prediction methodologies.

### **5.5 FLOOD PREDICTION IN DOWNSTREAM AREA IN LOWER ASSAM BY USING PRECIPITATION DATA OF PARTS OF MEGHALAYA HILLS IN THE UPPER CATCHMENT**

#### **5.5.1 Introduction**

Precipitation is a derived product of passive microwave remote sensing. It is one of the most vital information in the hydrology studies. Especially in case of heavy precipitation events, there are further consequences involved in the process, such as occurrence of flash flood, landslide etc. Precipitation information therefore is used by many remote sensing scientists to predict flash flood in neighbouring areas. One such

method developed for south western part of the state of Assam is discussed in the following.

### **5.5.2 Theoretical Background**

As discussed in the previous section, 5.4.2, the precipitation is measured by microwave satellites by correlating many terrestrial and atmospheric factors. This precipitation therefore is an important derived product, obtained from microwave satellites, which can be used as an indicating factor for flood prediction in the vulnerable areas.

### **5.5.3 Equipments and Data Used**

For the present work precipitation data is obtained from Advanced Microwave Scanning Radiometer (AMSR) 2 on board Global Change Observation Mission (GCOM) W1 satellite of Japan Aerospace Exploration Agency (JAXA). It is also understood that this real time data obtained, if timely utilized, can help in providing aids to decrease the human mortality rate. In the downloaded satellite precipitation image, the amount of precipitation in mm/h is available pixel-wise in it.

For analysing the precipitation images of the satellite, the ‘Beam-VISAT’ software provided by European Satellite Agency (ESA) is used. The results of the analysis are then stored in excel sheets for further calculations.

### **5.5.4 Study Area**

In the present study an algorithm is developed to assess the total precipitation values of the southern bank of the lower basin of the Brahmaputra valley in Assam, bordering Meghalaya. The places under study are shown in the map in Figure 5.20.



Figure 5.20: Places under study for prediction of flood in lower Assam

Analysis is done for the places extending from  $89.98^{\circ}\text{E}$  to  $91.3^{\circ}\text{E}$  and  $25.8^{\circ}\text{N}$  to  $26.1^{\circ}\text{N}$ . Precipitation data is collected from AMSR 2 for the ascending as well as descending passes of the satellite for the month of September, 2014.

### 5.5.5 Experiments Done

Precipitation data of the south bank of the lower basin of the river Brahmaputra up to the Assam-Meghalaya border was used for forecasting flash flood in the South-Western districts of Assam. The precipitation values obtained from the satellite for the points as shown in Figure 5.20 are then recorded for both ascending and descending passes of the satellite. Finally, a sum of the precipitation values is computed for all the points considered. High value of this sum is expected to serve as a prior indication of flash flood in the nearby low lying areas.

### 5.5.6 Results and Discussion

The precipitation values are presented in Tables 5.5 and 5.6 for ascending and descending passes of the satellite over lower Assam and Garo hills. Summing up of the

precipitation data shows that high values of precipitation were recorded on 21<sup>st</sup> and 22<sup>nd</sup> of September, 2014. The high values of precipitation obtained for the ascending pass of the satellite are for Rani, Assam it is 1026 mm/h, Rambrei, West Khasi Hills is 689 mm/h, Mawshynrut, West Khasi Hills is 950 mm/h, Riango, West Khasi Hills is 843 mm/h, Siejlieh, West Khasi Hills is 605 mm/h, Falafang, Kamrup, Assam is 592 mm/h, Hamaria Road, Boko is 518 mm/h and Bagdoba, Goalpara, Assam is 502 mm/h.

Figures 5.21 and 5.22 show the variation of sum of precipitation values as recorded by AMSR-2 for the selected areas during the satellite's descending as well as ascending passes respectively.

Table 5.5: Precipitation values obtained from AMSR 2 with respect to descending pass for the month of September, 2014 for selected places in lower Assam, West Khasi Hills and Garo Hills

Sl. No.	Places	Dates of September 2014								
		16	18	19	20	21	23	25	27	28
1	Samuka, Assam	0	0	0	0	166	0	0	0	0
2	Jalukbari, Assam	0	0	73	0	259	0	0	0	0
3	Nongstoin, West Khasi Hills	0	0	0	0	253	0	0	0	0
4	Gijang, West Khasi Hills	0	0	0	0	270	0	0	0	0
5	Hahim, Assam	0	0	0	0	278	0	0	0	0
6	Umshek, Khasi Hills	0	0	0	0	270	0	0	0	0
7	Falafang, Kamrup, Assam	0	0	29	0	246	0	0	0	0
8	Hamaria Road, Boko, Assam	0	0	0	24	272	0	0	0	0
9	Bagdoba,	0	0	0	0	260	0	0	0	0

	Goalpara, Assam									
10	Garbhanga, Assam	0	0	59	0	0	0	0	0	0
11	Bajendoba, North Garo Hills	0	0	0	0	0	0	0	0	0
12	Rani, Kamrup, Assam	0	0	0	0	875	0	0	0	0
13	Rambrei, West Khasi Hills	0	0	0	0	323	0	0	0	0
14	Mawshynrut, West Khasi Hills	0	0	40	0	260	0	0	0	0
15	Riangdo, West Khasi Hills	0	0	0	0	156	0	0	0	0
16	Siejlieh, West Khasi Hills	0	0	62	0	246	0	0	0	0
Summation of Precipitation Values		0	0	263	24	4134	0	0	0	0

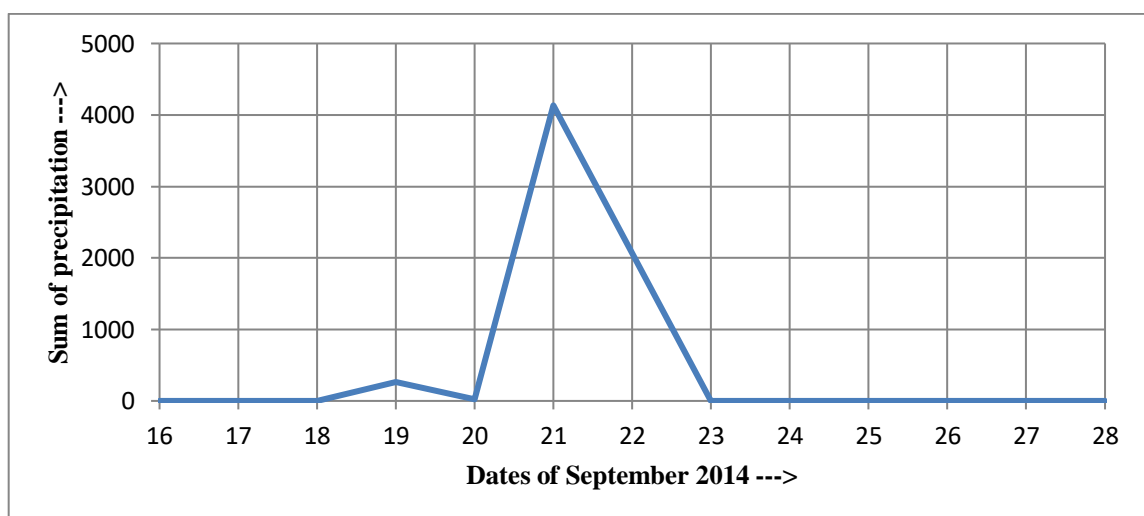


Figure 5.21: Sum of precipitation values obtained for the places in and around lower Assam area during descending pass of the satellite

Table 5.6: Precipitation values obtained from AMSR 2 with respect to ascending pass for the month of September, 2014 (lower Assam, West Khasi Hills and Garo Hills area)

Sl. No.	Places	Dates of September 2014						
		15	18	20	22	24	27	29
1	Samuka, Assam	0	0	0	0	0	0	0
2	Jalukbari, Assam	0	0	262	571	0	0	0
3	Nongstoin, West Khasi Hills	0	0	342	544	0	0	0
4	Gijang, West Khasi Hills	0	0	0	481	0	0	0
5	Hahim, Assam	0	0	35	471	0	0	0
6	Umshek, Khasi Hills	0	0	48	394	0	78	0
7	Falafang, Kamrup, Assam	0	0	71	592	0	0	0
8	Hamaria Road, Boko, Assam	0	0	0	518	0	0	0
9	Bagdoba, Goalpara, Assam	0	0	0	502	0	0	0
10	Garbhanga, Assam	0	0	430	476	0	0	0
11	Bajendoba, North Garo Hills	0	0	0	46	0	0	0
12	Rani, Kamrup, Assam	0	0	32	1026	0	0	0
13	Rambrei, West Khasi Hills	0	0	60	689	0	0	0
14	Mawshynrut, West Khasi Hills	0	0	0	950	0	0	0
15	Riangdo, West Khasi Hills	0	0	21	843	0	0	0
16	Siejlieh, West Khasi Hills	0	0	0	605	0	0	0
Summation of Precipitation Values		0	0	1301	8708	0	78	0

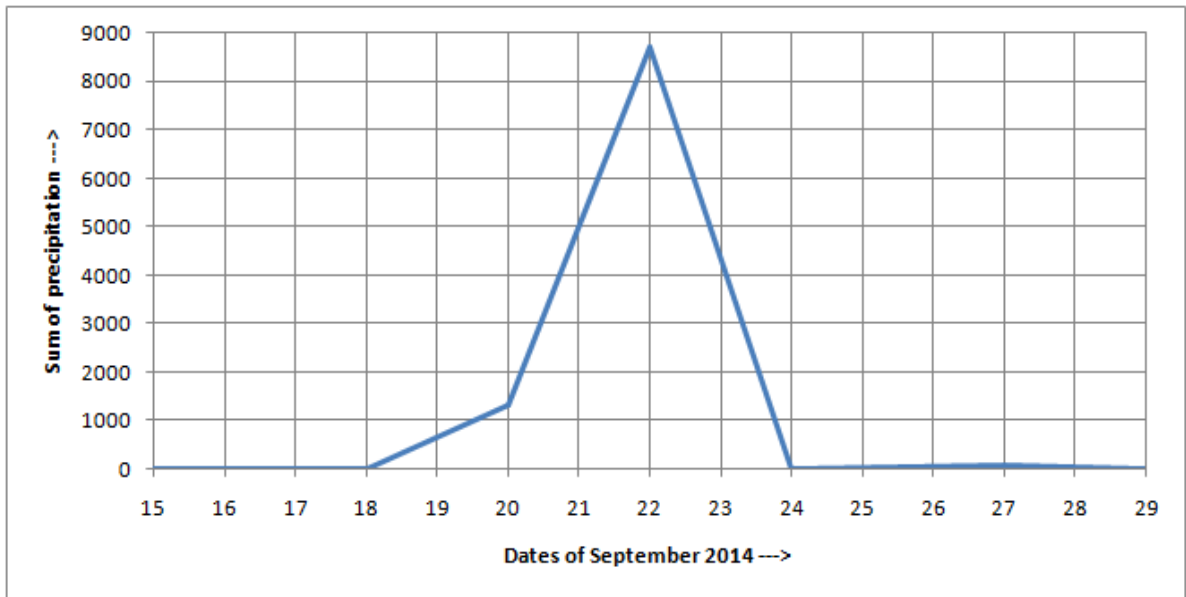


Figure 5.22: Sum of precipitation values obtained for the places in and around lower Assam area during ascending pass of the satellite

From Figures 5.21 and 5.22 it is observed that very high precipitation values have been recorded in the bordering areas of Assam and Meghalaya on the 21<sup>st</sup> and 22<sup>nd</sup> September, 2014.

### 5.5.7 Validation of the Experimental Results

From the experimental results it is seen that the heavy precipitation in the hilly areas such as- Rambrei, Mawshynrut, Riango, Siejlieh, Nongstoin, Gijang and Umshek has caused floods in the Goalpara and Kamrup districts of Assam. The rain water from the hilly areas flows down to the plains because of the terrain of the hilly areas. This heavy precipitation in the hills nearby has caused heavy inundation in the southern districts of Assam during 21<sup>st</sup> to 26<sup>th</sup> September, 2014, as recorded.

### **5.5.8 Inferences**

From the experimental results and the analyses it can be concluded that a record of high precipitation level observed by using AMSR 2 helps in forecasting of flood. Before the occurrence of a major flood, often very high precipitation values are recorded in nearby areas. It is seen in hilly areas like Assam-Meghalaya border, whenever precipitation magnitude is high in those areas, the water runs downhill due to the terrain and gets accumulated in the plain areas. In the south-western part of Assam, flood occurs frequently due to heavy rainfall in bordering Meghalaya hills.

Hence, it can be concluded that passive microwave remote sensors can play an important role in precipitation level monitoring and prediction of flood in the regions like the North Eastern region of India. By using this methodology, the precipitation values obtained from microwave remote sensing satellite can be utilized for prediction of flood, with a lead time of 1–4 days. The accuracy of such a method is found to be nearly 100 percent.

## **5.6 PREDICTION OF CLOUDBURST USING MICROWAVE REMOTE SENSING**

### **5.6.1 Introduction**

Cloudburst refers to the extreme form of precipitation, with a high amount of rainfall within a short span of time (100 mm or more rainfall per hour). This type of extreme rainfall often leads to flash flood, landslide and damage of infrastructure due to heavy rainfall. The loss of human lives is also not very uncommon due to sudden heavy downpour as well as flash flood caused by cloudburst. Hence, a prediction mechanism of such extreme form of precipitation needs to be developed using microwave remote sensing. This section presents a mechanism developed for prediction of cloudburst by detecting the formation of cumulonimbus type cloud using passive microwave remote sensed data.

### 5.6.2 Theoretical Background

Cloud and Rainfall affects earth emitted microwave radiation primarily in two ways, viz., absorption by rain drops, and scattering by ice particles. The scattering property is more prevalent at high frequencies and is caused by particles that are comparable in size to the wavelength of energy being measured. At 91 GHz, this translates to a particle size of about 4 mm or greater. In the rain layer in the atmosphere, there is a mixture of snow, ice and rain particles and this is the main cause of the scattering. This affect is detected by a decrease in  $T_B$  at higher frequencies, in the cloud covered regions.

$T_B$  values measured at 19 GHz and 91 GHz show variations due to both surface temperature ( $T_s$ ) and atmospheric emission ( $T_u$ ). However, the variation of  $T_B$  due to the presence of cloud is more prominent at 91 GHz, due to blocking of  $T_s$  and emission of  $T_u$ . This happens more when the water particle size on the cloud is larger, like in case of cumulonimbus type clouds, which is formed vertically in a tall but horizontally narrow formation. However, lower frequencies like 19 GHz are affected less by the cloud, due to their longer wavelength. Hence, the  $T_B$  difference between lower and higher frequencies is higher for a dense cloud covered sky. If the cloud is vertically formed with larger water droplets, then the  $T_B$  difference is even higher. This phenomenon is used as the characteristic criterion in the present work, for detection of cloud having the potential of causing very heavy rainfall, including cloudburst.

### 5.6.3 Equipments and Data Used

Following equipments and data are used for the study.

- (a) A PC with 'Beam VISAT' software for image processing and interpretation.
- (b) Brightness Temperature data of 19 and 91 GHz in horizontal polarization recorded during descending pass from SSMI/S sensors on board DMSP satellite.

### 5.6.4 Study Areas

The areas considered for testing of the algorithm developed for analysing the formation of cloud having the potential to cause cloudburst, are listed in Table 5.7. The table also shows the recorded dates of cloudburst events in those places. The areas selected for the study are from the states of Meghalaya, Jammu & Kashmir and Uttarakhand. Geographically the places are at very different locations in India; the latitudes and longitudes of the places being mentioned in the table. Hence, the surface characteristics of all these places are also of different types. However the main objective of the study is to consider the major cloudburst events reported across India from 2013 to 2016 and see the effectiveness of the developed methodology in predicting these events.

Table 5.7: Areas considered for detection of cloud capable of producing cloudburst

<i>Area of study</i>	<i>Latitude (°N)</i>	<i>Longitude (°E)</i>	<i>Recorded date of cloudburst</i>
South Garo Hills	25.2	90.6	September 21, 2014
Kashmir Valley	34.0	74.7	September 6, 2014
Tehri	30.4	78.5	July 31, 2014
Pithoragarh, Uttarakhand	30.1	80.4	July 1, 2016

### 5.6.5 Experiments Done

In the present study experiment is done with brightness temperature data recorded in the frequency level of 19, 22, 37 and 91 GHz during both ascending and descending passes of the satellite in horizontal and vertical polarizations. After experimentation it is found that the near real time  $T_B$  data at 19 and 91 GHz in horizontal polarization during descending pass can be more effectively used to detect formation of cloud having potential for heavy rainfall. Therefore, for predicting cloudburst, brightness temperatures in these two frequencies are only used. The sample brightness temperature images obtained from SSMI/S are shown in Figure 5.23.



Figure 5.23: Sample images containing  $T_B$  values at (a) 19 GHz and (b) 91 GHz

The methodology adopted for prediction of cloudburst by detecting heavy rainfall producing cloud is shown in Figure 5.24. First the  $T_B$  values are obtained from the images of 19 GHz and 91 GHz for the places under study. Then the difference in  $T_B$  values for a particular place is computed on different dates. The highly positive value of the  $T_B$  difference implies the presence of cloud, capable of producing cloudburst or very heavy rainfall. Low positive and negative values of the  $T_B$  difference indicate the absence of such cloud in the atmosphere. This methodology is adopted for overall analysis for detecting the presence of such cloud and thus for forecasting the occurrence of cloudburst and very heavy rainfall in advance.

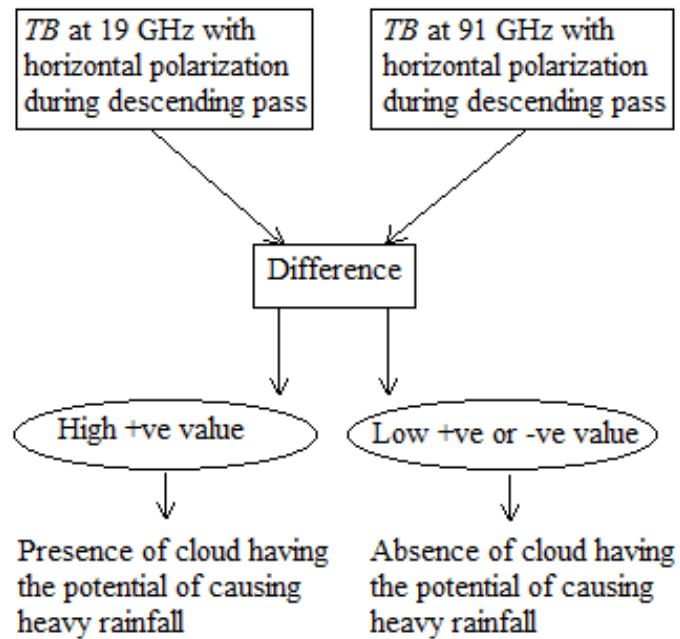


Figure 5.24: Methodology for detection of heavy rainfall producing cloud

### 5.6.6 Results and Discussion

The results obtained by following the methodology, for the places under study, are shown in the form of the graphs in Figures 5.25 to 5.28. From the figures it is seen that a high positive  $T_B$  difference value is obtained on certain dates, as compared to normal level.

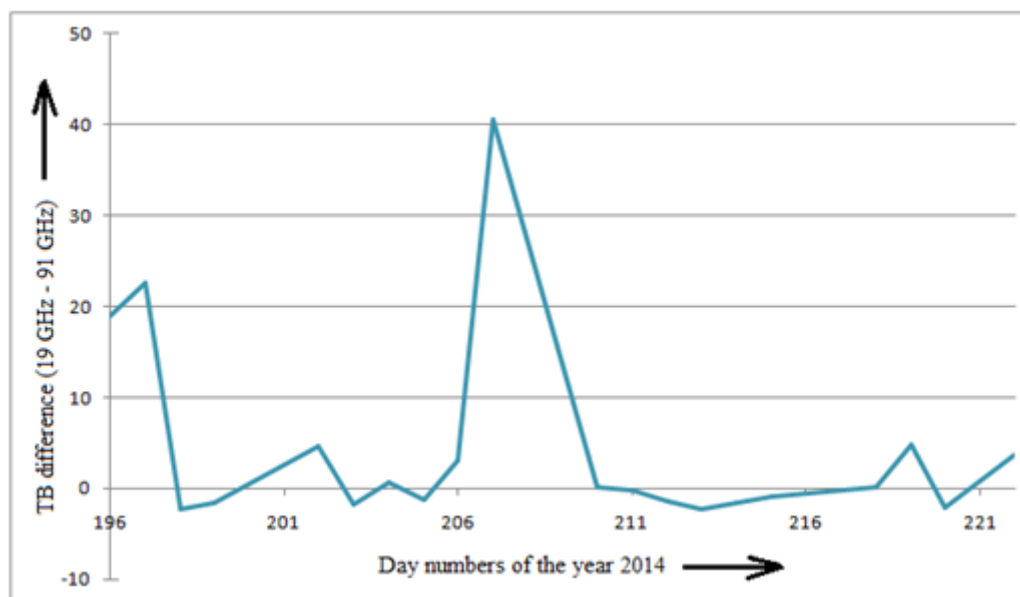


Figure 5.25: High positive value obtained on the 207<sup>th</sup> day (26<sup>th</sup> July) of 2014 for Tehri

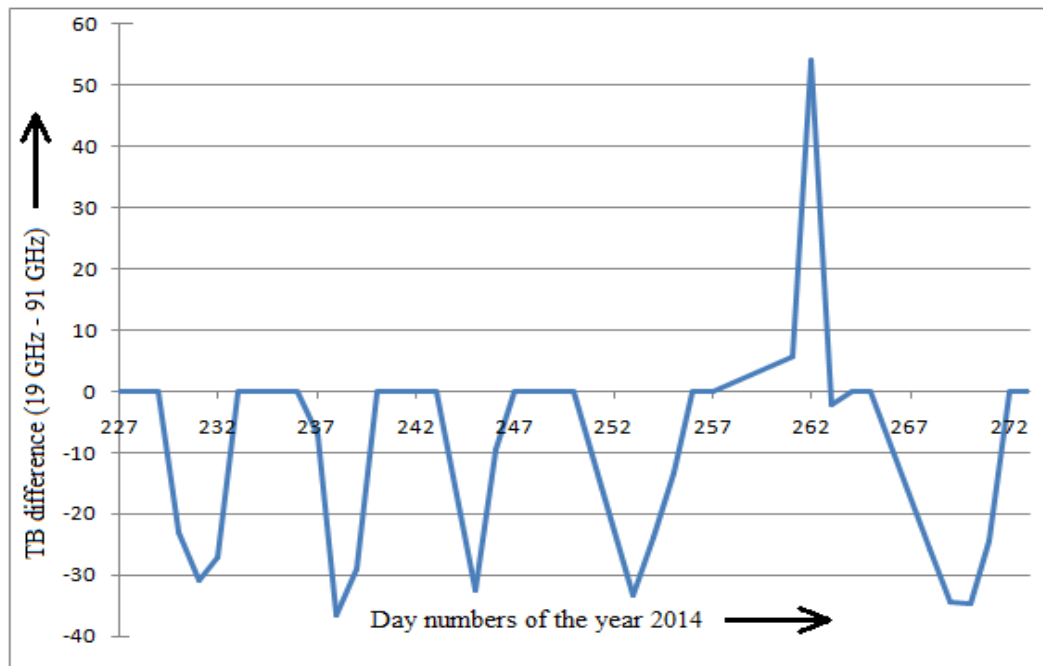


Figure 5.26: High positive value obtained on the 262<sup>nd</sup> day (19<sup>th</sup> September) of 2014 for South Garo Hills

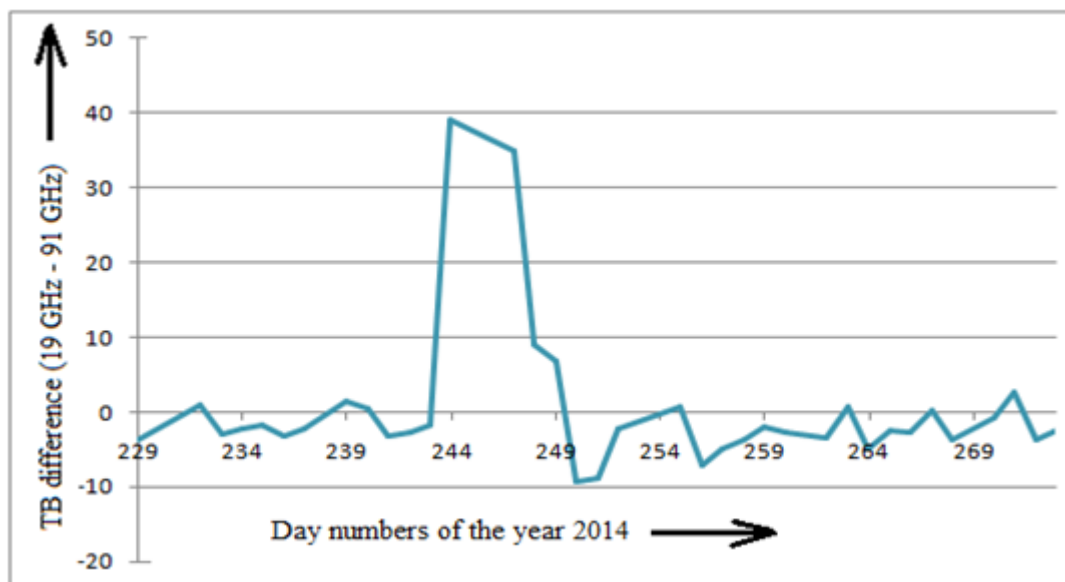


Figure 5.27: High positive value obtained from the 244<sup>th</sup> to 247<sup>th</sup> day (1<sup>st</sup> to 4<sup>th</sup> September) of 2014 for Kashmir Valley

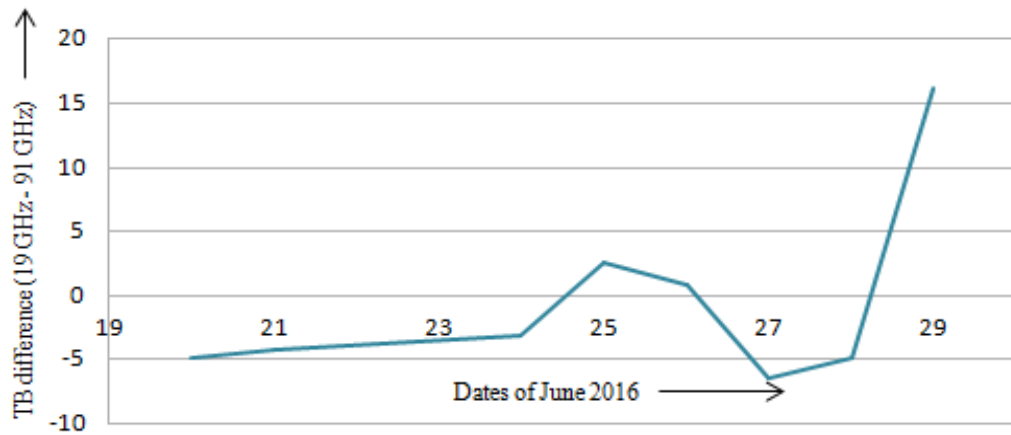


Figure 5.28: High positive value obtained on 29<sup>th</sup> June 2016, for Pithoragarh in Uttarakhand

For Tehri in Uttarakhand, the high positive value of  $T_B$  difference is obtained on 26<sup>th</sup> July. For South Garo Hills, Kashmir Valley and Uttarakhand also similar such high  $T_B$  difference values are obtained on certain days, possibly before the cloudburst occurrences.

As per the proposed methodology the high  $T_B$  difference can signify the presence of cloud having the potential of cloudburst, which is validated with the records of cloudburst from authentic sources on an immediately later date.

### 5.6.7 Validation of Experimental Results

The events of reported cloudburst at different locations are tabulated against the early warning dates obtained through the proposed methodology in Table 5.8.

Table 5.8: Actual Cloudburst dates against the early warning dates

<i>Location</i>	<i>Cloudburst Date</i>	<i>Early Warning Date</i>
Tehri	31.07.2014 [67]	26.07.2014
South Garo Hills	21.09.2014 [68]	19.09.2014
Kashmir	06.09.2014 [70]	01.09.2014 to 04.09.2014
Pithoragarh	01.07.2016 [71]	29.06.2016

This validates the proposed methodology of predicting the cloudburst and subsequent flooding in all the areas. The warning was obtained from the  $T_B$  difference values 2 to 5 days in advance.

### **5.6.8 Inferences**

The methodology described here for prediction of cloudburst by detecting the formation of cumulonimbus type cloud is found to be valid for all the four selected lower Himalayan regions in India. The methodology needs to be validated further by checking with other sets of past and future events of cloudburst in different regions of the world using data from variety of other microwave remote sensing satellites. The prediction of Cloudburst is an important indication of subsequent flash flood. All the four places where cloudburst occurred also reported flash flood immediately after the heavy downpour. Thus the brightness temperature difference is useful in predicting cloudburst as well as flash flood in any place with a lead time of 2 to 5 days.

## **5.7 CHAPTER CONCLUSIONS**

This chapter presents the flood prediction techniques successfully developed using passive microwave remote sensing methods as mentioned below.

- (1) Using Polarization Index- Use of this index for flood prediction is done for the first time, with a novel idea of selection of study areas in the Brahmaputra valley. The accuracy of prediction is about 80 percent, with a lead time of 1-3 days.
- (2) Using total Precipitation value- Use of the sum of precipitation upstream for flood prediction downstream is a novel idea successfully validated. Applying the same idea of finding the sum of precipitation in hill areas for predicting flood in the downstream riparian area has been successfully done with a lead time to 1-2 days and an accuracy of about 70 percent.

- (3) Using Brightness Temperature difference- Using this, a unique method of cloudburst prediction is developed with about 75 percent accuracy and with a lead time of 2-5 days.

The flood prediction methods developed are successfully tested and validated in a regional level. The region includes the state of Assam in general and the Brahmaputra valley to be precise. The cloudburst prediction methods are also validated for various other places in the country in order to ensure repeatability.